Experimental Section

Chemical and Materials

Pyrrole, methyl orange (MO), $FeCl_3$, $Co(NO_3)_2 \cdot 6H_2O$, 2-methylimidazole (2-MeIM), ethanol and methanol were purchased from Wako Pure Chemical Industries and used without further purification. NaCl, poly(vinylidene difluoride) (PVDF) and N-methyl 2-pyrrolidinone (NMP) was purchased from Sinopharm Chemical Reagent Co., Ltd. Vulcan XC 72 was purchased from Cabot Corporation.

Synthesis of PPy nanotubes

Firstly, 0.05 g of MO was thoroughly dispersed in 60 mL of deionized water. Then 0.243 g of $FeCl_3$ was added to the MO solution under intense stirring (300 rpm), cooled in an ice bath. After the inclusion of pyrrole (0.105 mL), the mixed solution was kept for 24 h under stirring (under dark conditions). Finally, the obtained precipitate was filtered and washed with a mixture of ethanol and water (for methyl orange elimination) several times and dried.

Synthesis of ZIF-67/PPy hybrid

40 mg of PPy nanotubes were first dispersed in 20 mL of methanol under ultrasonication for 1 h. Then 454 mg of $Co(NO_3)_2 \cdot 6H_2O$ was dispersed into the PPy nanotubes solution under stirring for 1 h to form a solution A. 513 mg of 2-MeIM was dissolved in 20 mL of methanol to form a solution B. Subsequently, solution B was added dropwise to solution A under sustained stirring for 30 min. After being kept still for 24 h, the precipitate was collected by centrifugation, washed thoroughly with methanol several times, and finally dried at 60 ºC for 24 h.

Materials characterization

The morphological characterizations were performed with a field-emission scanning electron microscope (FESEM, HITACHI SU-8230) operated at 5 kV. The interior structures were studied using a transmission electron microscope (TEM, JEOL JEM-2100F) working at an accelerating voltage of 200 kV. Powder X-ray diffraction (XRD) patterns were collected with an Ultima Rint 2000 X-ray diffractometer (RIGAKU, Japan). Fourier−transform infrared spectrum (FT-IR) spectrum was carried out by a Thermoscientific Nicolet 4700 FTIR Spectrometer using DTGS detector (wavenumber range: 400–4000 cm^{-1}). Nitrogen sorption isotherms were carried out using a BELSORP-mini (BEL, Japan). The specific surface area (SSA) was analyzed by Multipoint Brunauer-Emmett-Teller (BET) technique.

Electrochemical performance measurements

The electrode fabrication method is as follows: The electrode ink was prepared by mixing 80 wt% samples

with 10 wt% carbon black (Vulcan XC 72) and 10 wt% PVDF in NMP solvent under ultrasonication for 15 min. A certain volume of the ink was dropped onto the graphite paper with a thickness of 1 mm and dried at 60 °C for 12 h. The areal mass loading of each working electrode was 5 mg cm^{-2}.

The electrochemical performances were tested by cyclic voltammetry (CV) method performed on a CHI 660E electrochemical workstation using a three-electrode system with aqueous 1 M NaCl, platinum wire and Ag/AgCl electrode as the electrolyte, counter electrode and reference electrode, respectively. The Nyquist plots obtained from electrochemical impedance spectroscopy (EIS) were studied in a frequency range of 10 mHz to 100 kHz .

Calculation of specific capacitances derived from CV curves is according to the following equation:

$$C = \int idV \Big/ 2 \times \Delta V m v \tag{S1}$$

where i is the current (A), m is the mass of electrode materials (g), ΔV is the voltage window (V), and v is the scan rate (mV s^{-1}).

Desalination analyses by CDI

Each individual CDI electrode was fabricated by depositing a mixture of the sample with Vulcan XC 72 and PVDF binder on graphite paper (thickness: 1 mm). The weight ratio of sample, Vulcan XC 72, and PVDF was 8:1:1. The mixture was pressed onto graphite papers and dried in a vacuum oven at 60 °C for 12 h. Each electrode possessed a mass loading of about 10 mg cm^{-2}.

The CDI tests were conducted using a batch-mode with a continuous recycling system. For every individual experiment, the variance in concentration of the de-aerated NaCl solution was continuously recorded and measured by the ion conductivity meter. The volume was set at 50 mL, the flow rate was fixed at 20 mL min^{-1}, and the operating voltage was maintained at 1.2 V. The temperature was kept at 27 °C during measurement. The relationship between conductivity and concentration was obtained according to a calibration table made prior to the experiment.

To evaluate the desalination performance of ZIF-67/PPy hybrid, the CDI cell consisted of two pairs of parallel ZIF-67/PPy hybrid electrodes separated by a 200 μm thick nonconductive nylon cloth to prevent electrical short circuit and to act as a spacer channel. Additionally, anion- and cation- exchange membranes have also been used to alleviate the co-ion effect. The starting concentration of NaCl solution was about 584 mg L^{-1}, corresponding to ~10 mM .

To evaluate the practicability of ZIF-67/PPy hybrid for brackish water desalination, the CDI cell consisted of ten pairs of parallel ZIF-67/PPy hybrid electrodes. The concentration was about 1530 mg L^{-1}.

The desalination capacity (Γ, mg g^{-1}) and mean desalination rate (v, mg g^{-1} min^{-1}) at t min was calculated from the following equations:

$$\Gamma = (C_0 - C_t) \times V/m \quad \text{(S2)}$$

$$v = \Gamma/t \quad \text{(S3)}$$

where C_0 and C_t are the NaCl concentrations at initial stage and t min, respectively (mg L^{-1}), V is the volume of the NaCl solution (L), and m is the total mass of the electrode materials (g).

Adsorption kinetics, performed on the pseudo-first- and pseudo-second-order adsorption kinetic models, offers an useful tool to determine the rate constant and to analyze the adsorption process.[1-3] In the present work, pseudo-first- (S4) and pseudo-second-order (S5) kinetic models were utilized for the fitting of CDI data, respectively,

$$\log (q_e - q_t) = \log q_e - k_1 t/2.303 \quad \text{(S4)}$$

$$1/q_t = 1/k_2 q_e^2 t + 1/q_e \quad \text{(S5)}$$

where q_e and q_t represent the desalination capacity (mg g^{-1}) at equilibrium stage and time t (min). k_1 and k_2 represent the pseudo-first- and pseudo-second-order kinetic rate constants, respectively.

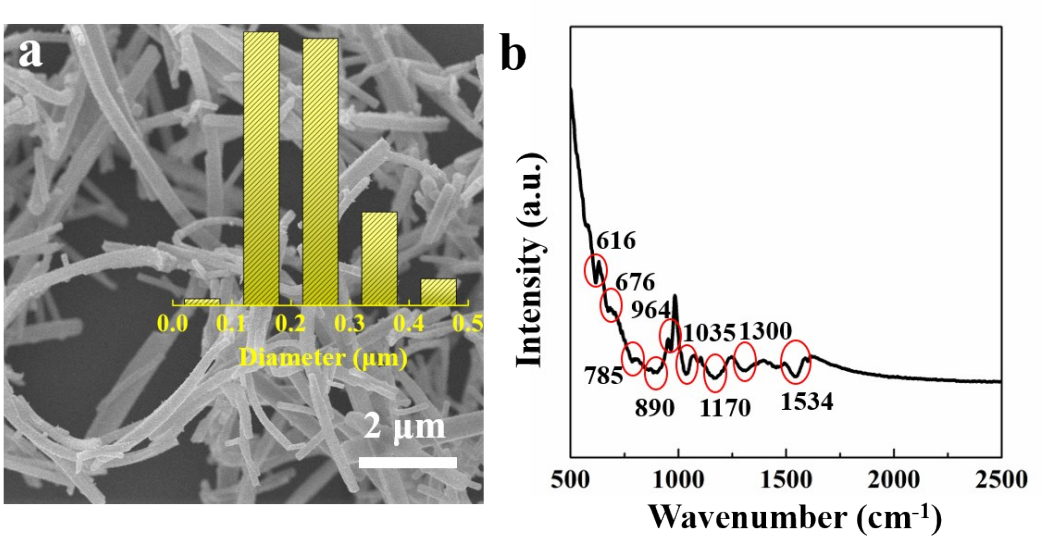

Fig. S1 (a) FESEM image and (b) FT-IR spectrum of PPy nanotubes.

Supplementary Note 1. The band at about 616 cm^{-1} belongs to the N-H out of plane vibration. The bands at 676 cm^{-1} and 785 cm^{-1} can be identified as the C-C out-of-plane ring deformation vibration and C-H out-of-plane ring deformation vibration, respectively. The band of the C-H out-of-plane deformation vibration of the ring appears at about 890 cm^{-1}. The C-C out-of-plane ring deformation vibration occurs at around 964 cm^{-1}. C-H and N-H in-plane deformation vibrations are responsible for the bands at 1035 and 1170 cm^{-1}, respectively. The broad bands at around 1300 cm^{-1} are attributed to C-H and C-N in-plane deformation vibrations. The band near 1534 cm^{-1} corresponds to the ring-stretching vibration.

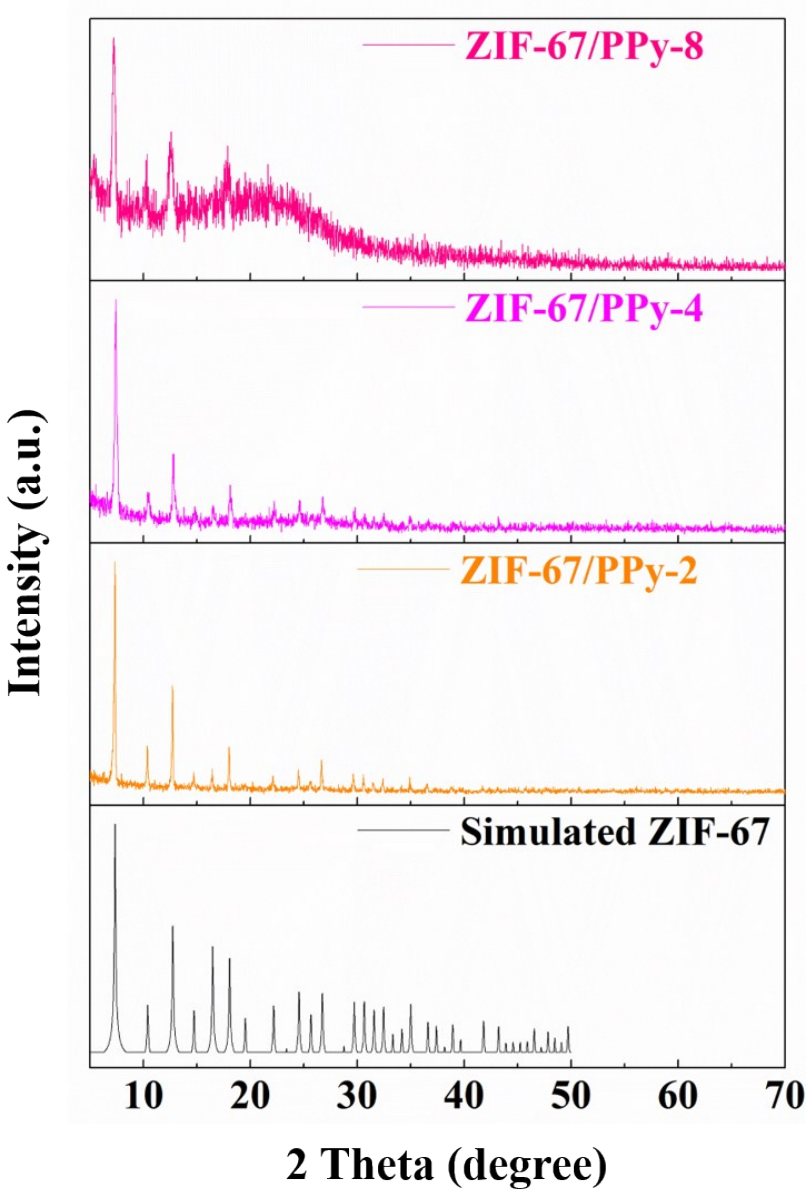

Fig. S2 XRD patterns of simulated ZIF-67, and ZIF-67/PPy-X (X=2, 4 and 8).

Supplementary Note 2. To clearly study the impact of amorphous PPy nanotubes on the structure of ZIF-67/PPy, we further increased the amount of PPy nanotubes to X-fold (X=2, 4 and 8) that of ZIF-67/PPy (the typical sample shown in Main text). The samples were abbreviated as ZIF-67/PPy-X (X=2, 4 and 8). As shown in **Fig. S2**, all samples show typical diffraction peaks of ZIF-67, and moreover, with further increasing the PPy content, the impact of PPy becomes obvious. But only at excessively high PPy content (increased up to 8-fold), the diffraction peaks of PPy nanotubes will be observed.

Table S1. R_{ct} values of PPy nanotubes, pure ZIF-67 and ZIF-67/PPy hybrid.

Sample	PPy nanotubes	ZIF-67	ZIF-67/PPy hybrid
R_{ct} (Ω)	0.62	3.20	1.32

Table S2. Comparison between ZIF-67/PPy hybrid with other EDL electrodes.

Sample	Specific surface area (m^2 g^{-1})	Voltage (V)	Desalination capacity (mg g^{-1})	Ref.
PAC/Cl	2652	1.2	5.8	4
ACP900	877	1.2	6.87	5
AC-1-2.0	2105	1.0	9.72	6
PCS1000	1321	1.6	5.81	7
AN-CFs	905.3	1.2	12.32	8
N-HPC	730	1.2	13.76	9
CCS	2680	1.2	16.1	10
PCNSs	2853	1.1	15.6	11
G@MC-O-thin	1270	1.5	24.3	12
mGE	474.0	1.2	14.2	13
Microporous graphene	3513	2.0	11.86	14
GTAC-20	426.56	1.2	10.94	15
GS	356.0	1.2	14.9	16
NC/rGO	1360	1.2	17.52	17
e-CNF-PCP	1450.6	1.2	12.56	18
PC-900	1911	1.2	10.90	19
ZIF-8@PZS-C	929	1.2	22.19	20
NC-800	798	1.2	8.52	21
PCP1200	1187.8	1.2	13.86	22
ZIF-67/PPy hybrid	1176.8	1.2	11.34	This work

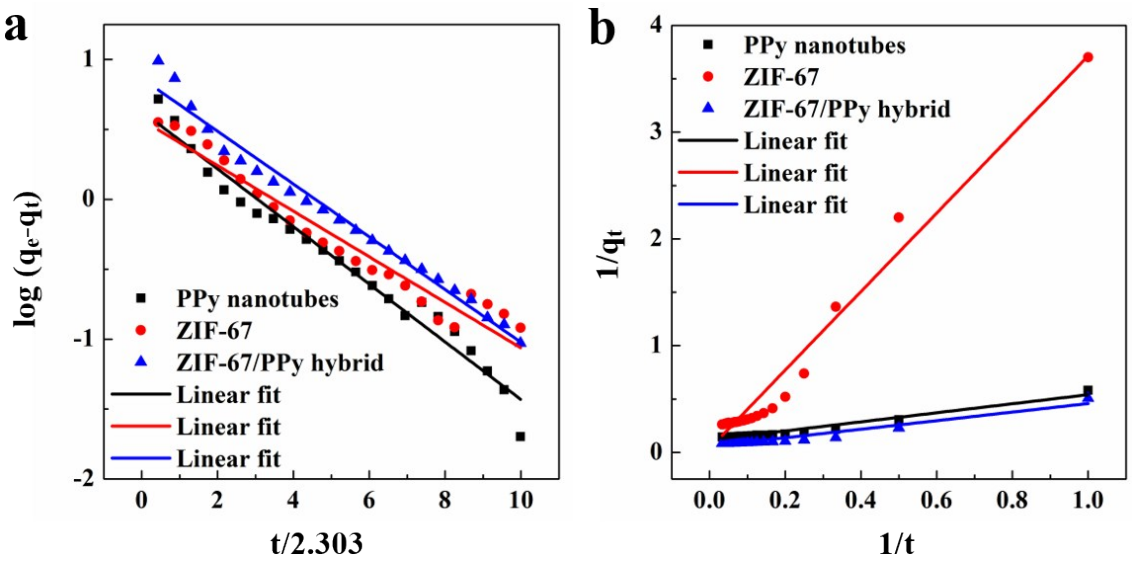

Fig. S3 The linear fittings for experimental data of the NaCl electrosorption using (a) pseudo-first- and (b) pseudo-second-order kinetic models.

Table S3. Coefficients of kinetic models for the electrosorption of PPy nanotubes, pure ZIF-67, and ZIF-67/PPy hybrid.

Sample		PPy nanotubes	ZIF-67	ZIF-67/PPy hybrid
Pseudo-first-order model	k_1	0.2062	0.1631	0.1887
	r^2	0.971	0.948	0.980
Pseudo-second-order model	k_2	3.25×10^{-2}	3.54×10^{-4}	8.28×10^{-3}
	r^2	0.958	0.969	0.936

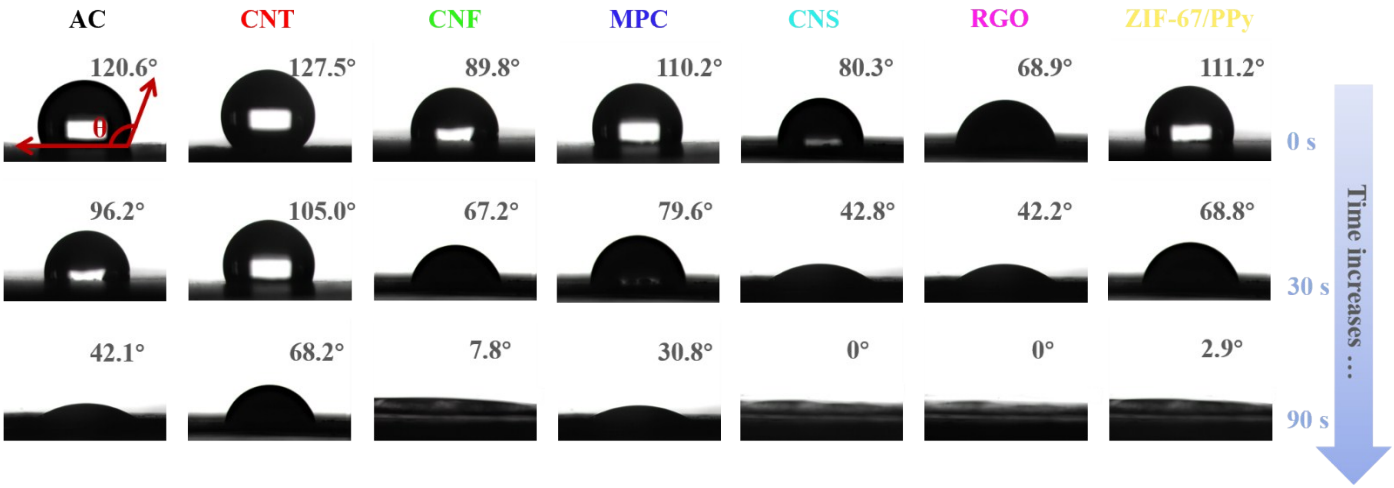

Fig. S4 Optical micrographs of the water contact angles on the surface of typical carbons (AC, CNT, CNF, MPC, CNS and RGO) and ZIF-67/PPy electrodes as a function of contact time.

References

1. J.-P. Simonin, *Chem. Eng. J.*, 2016, **300**, 254-263.
2. W. Tang, D. He, C. Zhang, P. Kovalsky and T. D. Waite, *Water Res.*, 2017, **120**, 229-237.
3. D. He, C. E. Wong, W. Tang, P. Kovalsky and T. D. Waite, *Environ. Sci. Technol. Lett.*, 2016, **3**, 222-226.
4. R. L. Zornitta, F. J. García-Mateos, J. J. Lado, J. Rodríguez-Mirasol, T. Cordero, P. Hammer and L. A. M. Ruotolo, *Carbon*, 2017, **123**, 318-333.
5. S. Rezma, I. B. Assaker, Y. litaiem, R. Chtourou, A. Hafiane and H. Deleuze, *Mater. Res. Bull.*, 2019, **111**, 222-229.
6. C.-L. Yeh, H.-C. Hsi, K.-C. Li and C.-H. Hou, *Desalination*, 2015, **367**, 60-68.
7. Y. Liu, L. Pan, T. Chen, X. Xu, T. Lu, Z. Sun and D. H. C. Chua, *Electrochim. Acta*, 2015, **151**, 489-496.
8. L. Zhang, Y. Liu, T. Lu and L. Pan, *J. Electroanal. Chem.*, 2017, **804**, 179-184.
9. Y. Li, I. Hussain, J. Qi, C. Liu, J. Li, J. Shen, X. Sun, W. Han and L. Wang, *Sep. Purif. Technol.*, 2016, **165**, 190-198.
10. G.-X. Li, P.-X. Hou, S.-Y. Zhao, C. Liu and H.-M. Cheng, *Carbon*, 2016, **101**, 1-8.
11. T. Wu, G. Wang, Q. Dong, F. Zhan, X. Zhang, S. Li, H. Qiao and J. Qiu, *Environ. Sci. Technol.*, 2017, **51**, 9244-9251.
12. O. Noonan, Y. Liu, X. Huang and C. Yu, *J. Mater. Chem. A*, 2018, **6**, 14272-14280.
13. X. Xu, Y. Liu, M. Wang, X. Yang, C. Zhu, T. Lu, R. Zhao and L. Pan, *Electrochim. Acta*, 2016, **188**, 406-413.
14. Z. Li, B. Song, Z. Wu, Z. Lin, Y. Yao, K.-S. Moon and C. P. Wong, *Nano Energy*, 2015, **11**, 711-718.
15. G. Zhu, W. Wang, X. Li, J. Zhu, H. Wang and L. Zhang, *RSC Adv.*, 2016, **6**, 5817-5823.
16. X. Xu, L. Pan, Y. Liu, T. Lu, Z. Sun and D. H. C. Chua, *Sci. Rep.*, 2015, **5**, 8458.
17. M. Wang, X. Xu, J. Tang, S. Hou, M. S. A. Hossain, L. Pan and Y. Yamauchi, *Chem. Commun.*, 2017, **53**, 10784-10787.
18. Y. Liu, J. Ma, T. Lu and L. Pan, *Sci. Rep.*, 2016, **6**, 32784.
19. X. Duan, W. Liu and L. Chang, *J. Taiwan Inst. Chem. E.*, 2016, **62**, 132-139.
20. J. Zhang, J. Fang, J. Han, T. Yan, L. Shi and D. Zhang, *J. Mater. Chem. A*, 2018, **6**, 15245-15252.
21. N.-L. Liu, S. Dutta, R. R. Salunkhe, T. Ahamad, S. M. Alshehri, Y. Yamauchi, C.-H. Hou and K. C. W. Wu, *Sci. Rep.*, 2016, **6**, 28847.
22. Y. Liu, X. Xu, M. Wang, T. Lu, Z. Sun and L. Pan, *Chem. Commun.*, 2015, **51**, 12020-12023.